

# Directed flow of light hadrons in Au+Au and isobar collisions at $\sqrt{s_{\text{NN}}} = 200$ GeV

Jing Jing,<sup>1</sup> Ze-Fang Jiang,<sup>1,2,\*</sup> C. B. Yang,<sup>2</sup> and Ben-Wei Zhang<sup>2</sup>

<sup>1</sup>*Department of Physics and Electronic-Information Engineering,  
Hubei Engineering University, Xiaogan, Hubei, 432000, China*

<sup>2</sup>*Institute of Particle Physics and Key Laboratory of Quark and Lepton Physics (MOE),  
Central China Normal University, Wuhan, Hubei, 430079, China*

The directed flow of light hadrons produced in Au+Au, Ru+Ru and Zr+Zr collisions at  $\sqrt{s_{\text{NN}}} = 200$  GeV, has been investigated in this paper. The development of tilted energy density, pressure gradient and radial flow along the  $x$ -direction, are systematically investigated within the viscous hydrodynamic model CLVisc. We compare the experimental data for identified light charged hadrons ( $\pi$ ,  $K$ ,  $p$ ) to Au+Au and isobar collisions at RHIC and find that counter-clockwise tilt of initial fireball is shown to be a vital source of the directed flow for final light hadrons. The tilted initial medium profile induces the positive/negative force by the average pressure gradient along the impact parameter ( $x$ ) direction at backward/forward rapidity, which leads to a negative slope of the  $x$  component of the QGP flow velocity with respect to rapidity ( $\eta_s$ ), and the same feature of the directed flow  $v_1$ . We further study the effect of nuclear structure on the directed flow, and find that the light hadrons  $v_1$  are insensitive to the nuclear deformation.

## I. INTRODUCTION

High energy nucleus-nucleus collisions performed at the Relativistic Heavy-Ion Collider (RHIC) and the Large Hadron Collider (LHC) suggest that a novel color-deconfined QCD matter (Quark-Gluon Plasma, known as QGP), is created in the reaction region. The azimuthally asymmetric flow (collective flow) of the observed hadrons in various collision systems [1–3] are important phenomena in study the strongly interacting nature of the QGP, such as directed flow  $v_1$ , elliptic flow  $v_2$ , triangular flow  $v_3$ , etc. It has been successfully described by relativistic hydrodynamic models [4–24], and the shear viscosity ratio ( $\eta_v/s$ ) extracted from the experimental data is suggested to be pretty small [25, 26].

The directed flow ( $v_1$ ) is one of earliest observables for investigating the collectivity properties in heavy ion collisions [27–29]. It is defined by the first-order Fourier coefficient of the final hadrons azimuthal distribution and has been widely investigated at both RHIC and LHC [30–37]. Lots of studies suggest that the directed flow is generated at very early stage in the nuclear collisions, whose typical time scale is nearly  $2R/\gamma$ , where  $R$  and  $\gamma$  being the nuclear radius and Lorentz boost factor, respectively [6, 27, 38]. Such a time scale is even before the produce time of the elliptic flow  $v_2$ . Therefore, directed flow  $v_1$  could be a useful probe to investigate the medium distribution and nucleon flow at the initial stage in nucleus-nucleus collisions [4, 30, 38–43]. There are lots of origins contributing to the directed flow of light hadron. Model calculations suggest that the  $v_1$  could depends on the deformation of the initial fireball geometry, the initial baryon density distribution, the flow velocity field, the equation of state of QGP medium, the external electromagnetic fields and also the final hadronic rescatterings [40, 44–51], although their exact quantitative contributions are still open and unsolved questions.

The recent isobar run of collisions of both  $^{96}_{44}\text{Ru}$  and  $^{96}_{40}\text{Zr}$  at

$\sqrt{s_{\text{NN}}} = 200$  GeV by the STAR Collaboration at RHIC [52] has a special motivation to search for the chiral magnetic field effect (CME) [53–56]. However, the isobar blind analysis did not provide predefined CME signal so far, but surprisingly found that  $^{96}_{44}\text{Ru} + ^{96}_{44}\text{Ru}$  collisions provided a higher particle yields than  $^{96}_{40}\text{Zr} + ^{96}_{40}\text{Zr}$  collisions as well as larger elliptic flow ( $v_2$ ), albeit having a smaller triangular flow ( $v_3$ ) [57, 58]. Those differences of experimental results at STAR indicate a difference in nuclear structure (geometry shape) whose observable effects are seemingly larger than those induced by the difference of the electric charge between  $^{96}_{44}\text{Ru}$  and  $^{96}_{40}\text{Zr}$  [52], and have been investigated from nuclear structure analyses by many studies [57, 59–65]. Therefore, it is of great interest to analyse a detailed comparison between  $^{96}_{44}\text{Ru}$  and  $^{96}_{40}\text{Zr}$  within a uniform QGP evolution framework, and identify the main features of the nuclear structure that contributed to the directed flow  $v_1$  of final state identified light hadron.

In this work, we utilise a tilted initial condition coupled with (3+1)-D viscous hydrodynamic model (CLVisc) [66–68] to investigate the origin of directed flow of light hadrons produced in Au+Au and isobar collisions at  $\sqrt{s_{\text{NN}}} = 200$  GeV, with nuclear structure parameters for Ru and Zr from the energy density functional theory (DFT) calculations [69–71]. The correlation between the fireball structure of the initial state and the directed flow coefficient of the final state light hadrons is presented. Our calculation find that the tilted initial energy density profile for different nucleus (Au, Ru and Zr) yields different non-zero average pressure gradient  $-\langle\partial_x P\rangle$  at forward/backward space-time rapidity. Which further induces a negative slope of the average flow velocity  $\langle v_x \rangle$  with respect to the space-time rapidity  $\eta_s$ , and finally the same size and sign of  $v_1$  vs.  $\eta$  for the light hadrons, which is consistent with the experimental data in Au+Au and isobar collisions at  $\sqrt{s_{\text{NN}}} = 200$  GeV [52, 72, 73]. In the end, we provide the directed flow ( $v_1$ ) comparison between three different nuclear structure for  $^{96}_{44}\text{Ru}$  and  $^{96}_{40}\text{Zr}$  nuclei.

This article is organized as follows. In Sec. II, we present the rapidity-dependent energy density distribution in Au+Au and isobar collisions and their impacts on the pressure gradient and flow velocity with respect to time during the hydrody-

\*Electronic address: [jiangzf@mails.ccnuc.edu.cn](mailto:jiangzf@mails.ccnuc.edu.cn)

dynamic simulations. In Sec. III, we present the directed flow of light hadrons from our hydrodynamic calculation and study its dependence on the nuclear structure. We present a brief summary in Sec. IV.

## II. THE MODEL FRAMEWORK

### A. Parametrization of longitudinal profiles for energy density

In order to investigate the directed flow of light hadrons in Au+Au and isobar collisions, following our previous works [74–77], we start with construct the initial energy density distribution for nucleus Au, Ru and Zr. Their impacts on the pressure gradient and flow velocity with respect to time will be investigated using the (3+1)-D hydrodynamic model CLVisc.

Based on the Woods-Saxon (WS) distribution, the nucleus thickness function is defined as

$$T(x, y) = \int_{-\infty}^{\infty} dz \frac{n_0}{1 + \exp\left[\frac{r - R_0(1 + \beta_2 Y_2^0(\theta))}{d}\right]}, \quad (1)$$

where  $r = \sqrt{x^2 + y^2 + z^2}$  is the radial position with  $x$ ,  $y$ ,  $z$  are the space coordinates,  $\theta$  is polar angle in their rest frame,  $d$  is the surface diffusiveness parameter,  $\beta_2$  is the quadruple deformity of nucleus,  $Y_2^0(\theta) = \frac{1}{4}\sqrt{\frac{5}{\pi}}(3\cos^2\theta - 1)$  and  $R$  is the radius of the nuclear, which depends on the nucleus species. The parameters used for Au, Ru and Zr in the current study are listed in Tab. I. At present, nuclear density distribution of  $^{96}_{44}\text{Ru}$  and  $^{96}_{40}\text{Zr}$  are not accurately confirmed, because there are numbers of setups of parameters ( $R_0$ ,  $d$  and  $\beta_2$ ) from different experiments and models. In this work, following the pioneering work [69–71] and STAR experiment [52], we first adopt the nuclei sets from recent calculations based on energy density functional theory (DFT) [69–71, 78] to study the light hadron directed flow. And other two sets will be discussed later when we investigated the effect of nuclear structure on the directed flow  $v_1$  of final light hadrons.

Nucleus	$n_0$ [1/fm <sup>3</sup> ]	$R_0$ [fm]	$d$ [fm]	$\beta_2$
$^{197}_{79}\text{Au}$	0.17	6.38	0.535	0.0
$^{96}_{44}\text{Ru}$	0.16	5.067	0.500	0.0
$^{96}_{40}\text{Zr}$	0.16	4.965	0.556	0.0

TABLE I: Nuclear parameters used in the Woods-Saxon distribution for Au, Ru and Zr [52, 79].

Considering the projectile and target nuclei propagate along  $\pm\hat{z}$  direction with the impact parameter  $\mathbf{b}$ , the corresponding thickness function can be written as

$$T_+(\mathbf{x}_T) = T(\mathbf{x}_T - \mathbf{b}/2), \quad T_-(\mathbf{x}_T) = T(\mathbf{x}_T + \mathbf{b}/2), \quad (2)$$

where  $\mathbf{x}_T = (x, y)$  is the transverse plane coordinate. The density distributions of the participant nucleons are then given

by

$$T_1(\mathbf{x}_T) = T_+(\mathbf{x}_T) \left\{ 1 - \left[ 1 - \frac{\sigma_{\text{NN}} T_-(\mathbf{x}_T)}{A} \right]^A \right\}, \quad (3)$$

$$T_2(\mathbf{x}_T) = T_-(\mathbf{x}_T) \left\{ 1 - \left[ 1 - \frac{\sigma_{\text{NN}} T_+(\mathbf{x}_T)}{A} \right]^A \right\}, \quad (4)$$

where  $A$  is the nuclei mass number,  $\sigma_{\text{NN}} = 42$  mb is the inelastic nucleon-nucleon scattering cross section at  $\sqrt{s_{\text{NN}}} = 200$  GeV [79]. The centrality bin in different nuclear collisions are determined by the impact parameter  $\mathbf{b}$  [79].

Since the right/left-moving wounded nucleons (as shown in Fig. 1) are expected to emit more particles at forward/backward rapidity. We assume this can be constructed by introducing a deformation mechanism into the weight function  $W_N$  [74]. In which a tilted fireball is obtained to describing the observed charged particle directed flow at RHIC and LHC energy region [74, 80]. In our earlier studies [74–76], a monotonic function ( $T_1(x, y) + T_2(x, y)$ ) was introduced to obtain the asymmetric contribution between the forward and backward nucleus as follow,

$$W_N(x, y, \eta_s) = T_1(x, y) + T_2(x, y) + H_t [T_1(x, y) - T_2(x, y)] \tan\left(\frac{\eta_s}{\eta_t}\right), \quad (5)$$

where  $H_t$  reflects the strength of imbalance at the forward and backward rapidities, the function  $\tan(\eta_s/\eta_t)$  produces the deformation of the initial energy density distribution along the longitudinal direction, and  $\eta_t = 8.0$  is utilized for all the collision systems [74].

The initial energy density  $\varepsilon(x, y, \eta_s)$  is given by [67]

$$\varepsilon(x, y, \eta_s) = K \cdot W(x, y, \eta_s) \cdot H(\eta_s), \quad (6)$$

where  $K$  is a normalization factor and determined by the multiplicity density distribution ( $dN_{\text{ch}}/d\eta$ ) of soft particles. The total weight function  $W(x, y, \eta_s)$  is defined as

$$W(x, y, \eta_s) = \frac{0.95W_N(x, y, \eta_s) + 0.05n_{\text{BC}}(x, y)}{[0.95W_N(0, 0, 0) + 0.05n_{\text{BC}}(0, 0)]|_{\mathbf{b}=0}}. \quad (7)$$

Here, the number of binary collisions  $n_{\text{BC}}(x, y)$  is defined as [67, 79]

$$n_{\text{BC}}(x, y) = \sigma_{\text{NN}} T_+(x, y) T_-(x, y). \quad (8)$$

Additionally, in Eq. (6), a function

$$H(\eta_s) = \exp\left[-\frac{(|\eta_s| - \eta_w)^2}{2\sigma_\eta^2} \theta(|\eta_s| - \eta_w)\right] \quad (9)$$

is introduced to describe the plateau structure of the rapidity distribution of emitted hadrons at mid-rapidity, in which  $\eta_w = 1.3$  determines the width of the central rapidity plateau while  $\sigma_\eta = 1.5$  determines the width (speed) of the Gaussian decay from the plateau region [67].

In Tab. II, we summarize the parameters of initial conditions that are tuned to provide reasonable descriptions of the charged particles yields in the most central collisions [67], as will be shown in Fig. 6. They including, overall normalization factor ( $K$ ), the initial time of the hydrodynamic evolution ( $\tau_0$ ), the impact parameters ( $b$ ) and the tilted parameters ( $H_t$ ).

Parameters	Au+Au	Ru+Ru	Zr+Zr
$K$ (GeV/fm <sup>3</sup> )	35.5	23.0	23.0
$\tau_0$	0.6	0.6	0.6
$b$	2.4	2.1	2.1
$H_t$	1.0	1.0	1.0

TABLE II: Parameters used in hydrodynamic simulations between different nucleus [67, 74, 75, 79].

In present work, we set the initial fluid velocity in the transverse and space-time rapidity directions following the Bjorken approximation, i.e.,  $v_x = v_y = 0$  and  $v_z = z/t$ .

### B. Tilted energy density, eccentricity and pressure gradient

Using the tilted initial conditions above, we first present the energy density profile between different nucleus (Au, Ru and Zr). In Fig. 1, we present the energy density profile for 50-80% Au+Au, Ru+Ru and Zr+Zr collisions at  $\sqrt{s_{NN}} = 200$  GeV in the  $\eta_s - x$  plane. Here the model parameter  $H_t = 4.5$  is taken for the Au+Au collisions (top panel) and  $H_t = 3.9$  for the Ru+Ru collisions (middle panel), while  $H_t = 3.1$  for Zr+Zr collisions (bottom panel). In which  $H_t$  are extracted from experimental data to describe the directed flow  $v_1$  of charged particles and protons/anti-protons. From Fig. 1, we find that the energy density distribution for different nucleus is not only shifted in the forward/backward rapidity direction, it is also tilted counter-clockwise with respect to  $x = 0$  [74, 80].

For the purpose of quantify the asymmetry strength of the initial energy density for different nucleus at initial state, we first present the first-order eccentricity coefficient  $\varepsilon_1$  as a function of the space-time rapidity in Fig. 2. The first-order eccentricity vector  $\vec{\mathcal{E}}_1$  is defined as [15, 47]:

$$\vec{\mathcal{E}}_1 \equiv \varepsilon_1(\eta_s) e^{i\Psi_1(\eta_s)} = -\frac{\int d^2r \tilde{r}^3 e^{i\tilde{\phi}} \varepsilon(r, \phi, \eta_s)}{\int d^2r \tilde{r}^3 \varepsilon(r, \phi, \eta_s)}, \quad (10)$$

where the angular distribution is calculated with respect to the energy density weighted center-of-mass point  $(x_0(\eta_s), y_0(\eta_s))$  in every rapidity slice given by

$$x_0(\eta_s) = \frac{\int d^2r x \varepsilon(r, \phi, \eta_s)}{\int d^2r \varepsilon(r, \phi, \eta_s)}, \quad (11)$$

$$y_0(\eta_s) = \frac{\int d^2r y \varepsilon(r, \phi, \eta_s)}{\int d^2r \varepsilon(r, \phi, \eta_s)}, \quad (12)$$

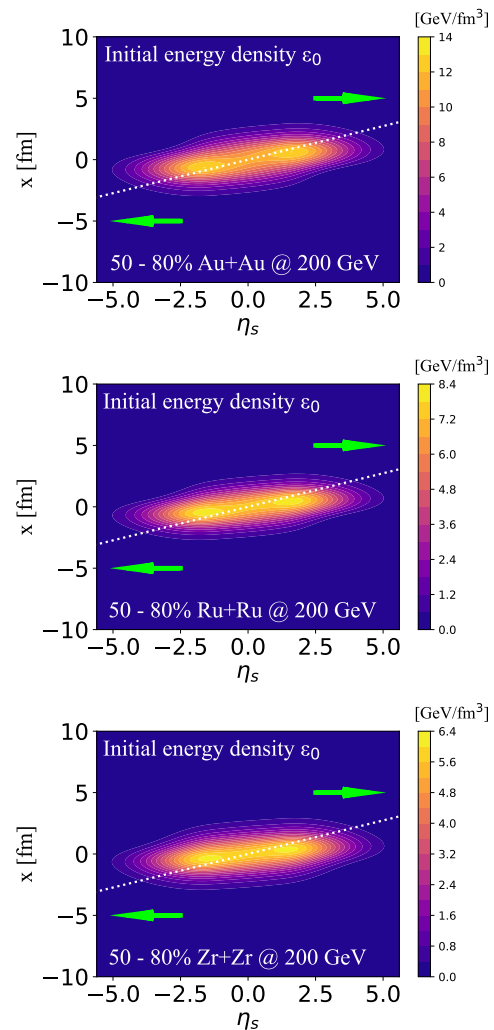


FIG. 1: (Color online) The initial tilted energy density on the  $\eta_s$ - $x$  plane at  $\tau_0 = 0.6$  fm/c in 50-80% Au+Au ( $b = 11.4$  fm), Ru+Ru ( $b = 9.3$  fm) and Zr+Zr ( $b = 9.6$  fm) collisions at  $\sqrt{s_{NN}} = 200$  GeV. The dotted line (snow color) show the counter-clockwise tilted initial condition with respect to the  $x = 0$  axis in the  $\eta_s$ - $x$  plane, and the arrow (lime color) sketch the moving at forward and backward rapidity.

where  $\tilde{r}(x, y, \eta_s) = \sqrt{(x - x_0)^2 + (y - y_0)^2}$  is the transverse radius and  $\tilde{\phi}(x, y, \eta_s) = \arctan[(y - y_0)/(x - x_0)]$  is the azimuthal angle, respectively. Please note that  $\varepsilon_1$  in Eq. (10) presents the first-order eccentricity coefficient and  $\Psi_1$  gives the corresponding participant plane angle. The  $\vec{\mathcal{E}}_1$  with respect to  $\eta_s$  contributes to explaining what kind of tilted fireball is needed to produce the light hadron  $v_1$ .

In Fig. 2, we present the  $\varepsilon_1$  as a function of space-time rapidity in 50-80% Au+Au and isobar collisions at  $\sqrt{s_{NN}} = 200$  GeV, they are odd functions of space-time rapidity  $\eta_s$  and positive/negative in the  $+/-\eta_s$  region. The slope of  $\varepsilon_1$  for three nucleus are larger than 0 at mid-rapidity but flipped within  $|\eta_s| > 1.5$ . This will further affect the evolution of the nu-

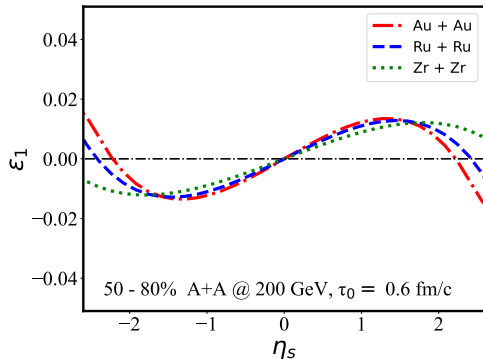


FIG. 2: (Color online) The first-order eccentricity coefficient  $\varepsilon_1(\eta_s)$  in 50-80% nucleus-nucleus collisions at  $\sqrt{s_{NN}} = 200$  GeV.

clear medium in the hydrodynamic simulation.

In addition to the initial energy density profile along the rapidity direction, we also present the initial pressure gradient  $-\partial_x P$  in the transverse plane, which directly drives the radial flow of nuclear matter. In Fig. 3, the initial  $-\partial_x P$  distribution in the  $x$ - $y$  plane at a fixed forward rapidity  $\eta_s = 1.2$  is presented for nucleus Au, Ru and Zr, where the same parameter values of  $H_t$ ,  $b$  are used for Fig. 1. One may clearly find the positive/negative value of pressure gradient  $-\partial_x P$  in the  $+/-x$  direction that leads to the outward expansion of the nuclear medium. From the top to bottom panels, we see that at  $\eta_s = 1.2$ , the center (zero pressure) regions of these distributions are shifted towards  $+x$  due to the counter-clockwise tilt of the initial energy density. Whether the average  $x$ -component of the final-state hadron momentum will be positive or negative at a given rapidity depends on the average magnitude of  $-\partial_x P$  in the corresponding transverse plane and how it evolves with time. This will be presented later in this work.

### C. Hydrodynamic evolution of the QGP

Using the tilted initial condition described above, we utilize the viscous hydrodynamic model CLVisc [66–68, 81, 82] to simulate the evolution of the QGP medium. The hydrodynamic equation satisfies [22, 83–86]

$$\partial_\mu T^{\mu\nu} = 0, \quad (13)$$

where  $T^{\mu\nu}$  is the energy-momentum tensor and take the following form:

$$T^{\mu\nu} = \varepsilon u^\mu u^\nu - (P + \Pi)\Delta^{\mu\nu} + \pi^{\mu\nu}. \quad (14)$$

Here  $\varepsilon$  is the energy density,  $u^\mu$  is the fluid four-velocity field,  $P$  is the pressure,  $\pi^{\mu\nu}$  is the shear stress tensor and  $\Pi$  is the bulk pressure. The projection tensor satisfied  $\Delta^{\mu\nu} = g^{\mu\nu} - u^\mu u^\nu$ , and the metric tensor  $g^{\mu\nu} = \text{diag}(1, -1, -1, -1)$ . In this work, we utilize the lattice QCD Equation of State (EoS) from the Wuppertal-Budapest group (2014) [87], and

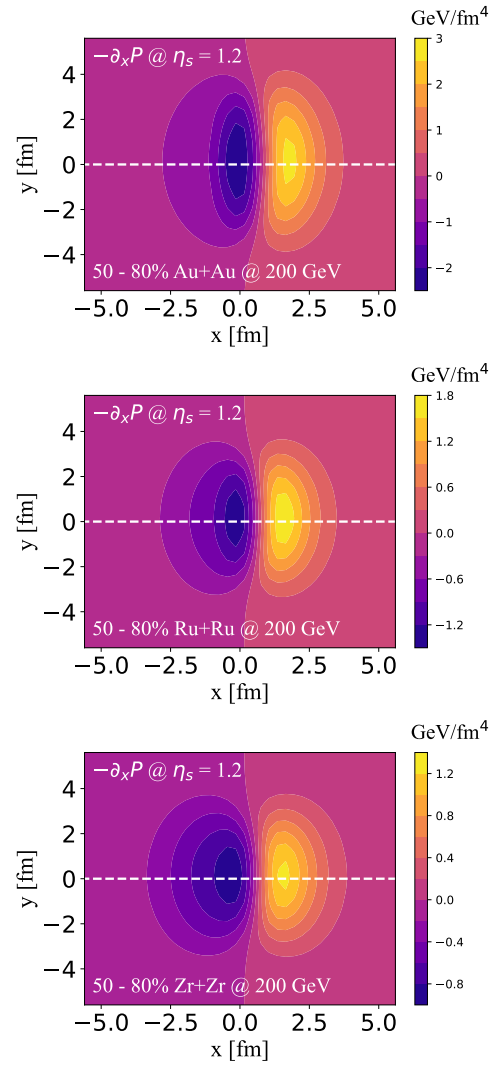


FIG. 3: (Color online) The pressure gradient  $-\partial_x P$  on the  $x$ - $y$  plane at initial proper time  $\tau_0 = 0.6$  fm/c in 50-80% Au+Au and isobar collisions.

the shear viscosity ratio is set as  $\eta_v/s = 0.08$  ( $\eta_v$  for the shear viscosity) for all collision systems. Follow the recent studies [74, 75], the bulk viscosity and net baryon density are ignored at this moment, and will also be taken into account in our future work [88, 89].

When the local temperature of nuclear matter drops below the freeze-out temperature (we set  $T_{fz} = 137$  MeV) [67], the Cooper-Frye mechanism [90] is used to calculate the spectra of hadrons on the freeze-out hypersurface. Contributions from resonance decay are taken into account according to our previous work [74, 75].

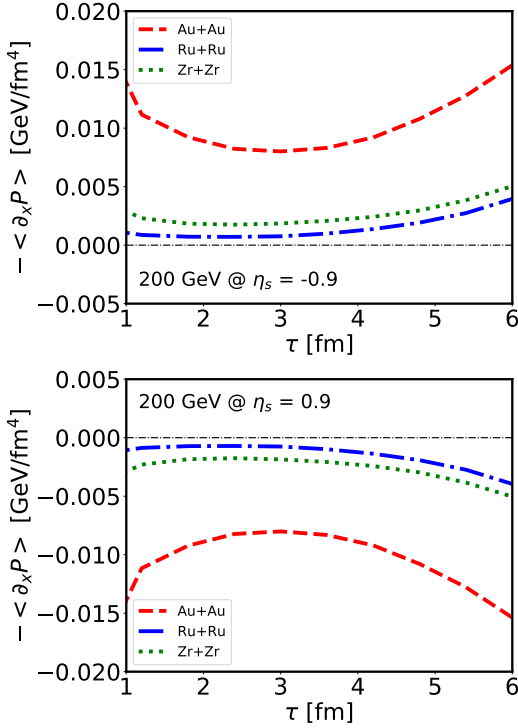


FIG. 4: (Color online) Time evolution of the average pressure gradient in the  $x$  direction at  $\eta_s = -0.9$  (upper panel) and  $\eta_s = 0.9$  (lower panel) in 50-80% Au+Au and isobar collisions at  $\sqrt{s_{\text{NN}}} = 200$  GeV.

#### D. Evolution of average pressure gradient and flow velocity with respect to proper time

Hydrodynamic simulation presents how the imbalance of the initial energy density distribution is developed to the anisotropy of the final-state hadron momentum. In this subsection, we present how the fluid velocity  $\langle v_x \rangle$  develops with respect to time at opposite rapidity  $\eta_s$ . This will help us observe the development of directed flow  $v_1$  and how it depends on the initial tilted geometry of the energy density.

As presented in Fig. 3 above, the tilted initial energy density leads to asymmetry of the pressure gradient along the  $x$  direction. In Fig. 4, we present how the average pressure gradient  $-\langle \partial_x P \rangle$  evolves with time at a given  $\eta_s$  ( $\pm 0.9$  here) in 50-80% Au+Au and isobar collisions at  $\sqrt{s_{\text{NN}}} = 200$  GeV. One may clearly observe that the evolution of  $-\langle \partial_x P \rangle$  is significantly affected by the tilted initial energy density distribution. The  $-\langle \partial_x P \rangle$  is keeping positive with time at  $\eta_s = -0.9$  while keeping negative at  $\eta_s = 0.9$ , leading to a continuous force that accelerates the QGP medium outward expansion toward the  $+x$  direction at  $\eta_s = -0.9$  while toward the  $-x$  direction at  $\eta_s = 0.9$ . Little difference is obtained between the isobar Zr and Ru. We note that unlike higher-order components of anisotropy, the first order eccentricity coefficient  $\varepsilon_1$  and pressure gradient  $-\langle \partial_x P \rangle$  are not necessarily positively correlated to each other.

Due to the tilted deformation of nuclear matter, medium ex-

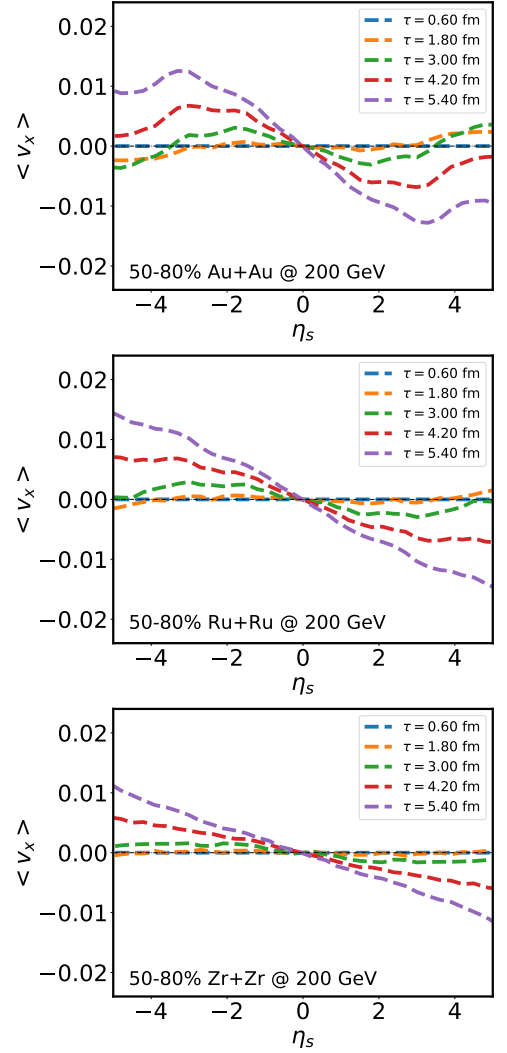


FIG. 5: (Color online) Space-time rapidity dependence of the average flow velocity in the  $x$  direction at different evolution times in 5-40% Au+Au collisions at  $\sqrt{s_{\text{NN}}} = 200$  GeV, compared between three parametrization methods of the initial condition.

pansion contributes to an overall force toward the  $+/-x$  direction at backward/forward rapidity. A direct outcome of such force is the asymmetric flow velocities in the corresponding direction. In Fig. 5, we present how the average flow velocity  $\langle v_x \rangle$  develops with time. The average flow velocity at a given proper time and space-time rapidity is defined as [16, 45],

$$\langle v_x(\eta_s) \rangle = \frac{\int d^2r v_x \gamma \varepsilon(r, \phi, \eta_s)}{\int d^2r \gamma \varepsilon(r, \phi, \eta_s)}, \quad (15)$$

where  $\gamma = 1/\sqrt{1 - v_x^2 - v_y^2 - v_z^2}$  is the Lorentz boost factor.

In Fig. 5, one observes that the average flow velocity  $\langle v_x \rangle$  is positive/negative at backward/forward rapidity. The magnitude of  $\langle v_x \rangle$  increases with time due to the non-zero pressure gradient  $-\langle \partial_x P \rangle$ . One finds that a larger  $|\langle \partial_x P \rangle|$  leads

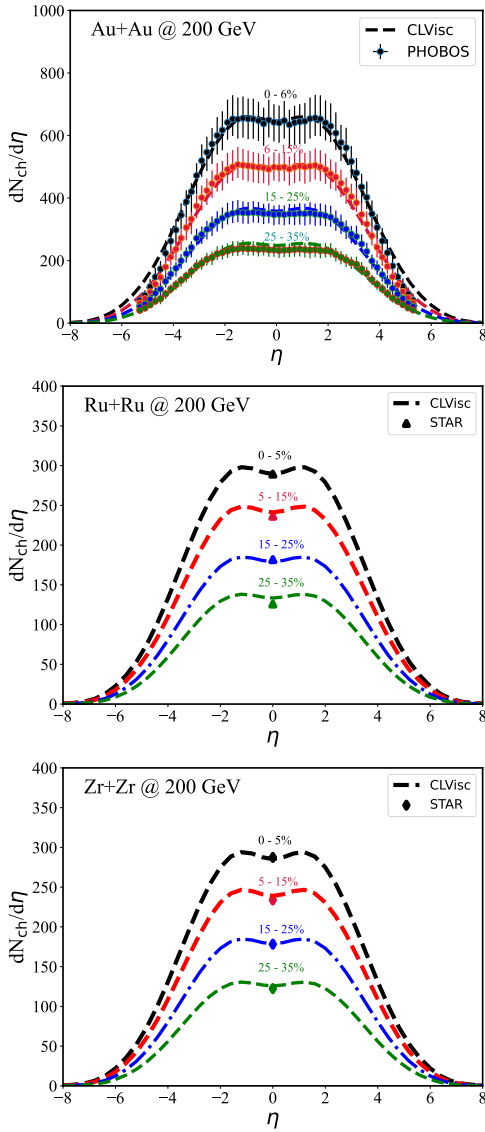


FIG. 6: (Color online) Pseudorapidity distribution of charged light hadrons in Au+Au and isobar collisions at  $\sqrt{s_{\text{NN}}} = 200$  GeV, compared between the CLVisc hydrodynamic calculation with three nucleus and the PHOBOS and STAR data [52, 91].

to a larger  $\langle v_x \rangle$  at  $|\eta_s|$  around  $|\eta_s| \approx 2$  regime than around  $|\eta_s| \approx 1$  regime. The average flow velocity  $\langle v_x \rangle$  here will directly produce the directed flow of the light hadrons.

### III. NUMERICAL RESULTS

In this section, we present the numerical results for light hadrons yield and directed flow in Au+Au and isobar collisions at  $\sqrt{s_{\text{NN}}} = 200$  GeV using the above tilted initial condition and hydrodynamic model CLVisc. In particular, we investigate how the directed flow depends on the effect of nuclear structure of the isobar  $^{96}_{44}\text{Ru}$  and  $^{96}_{40}\text{Zr}$ .

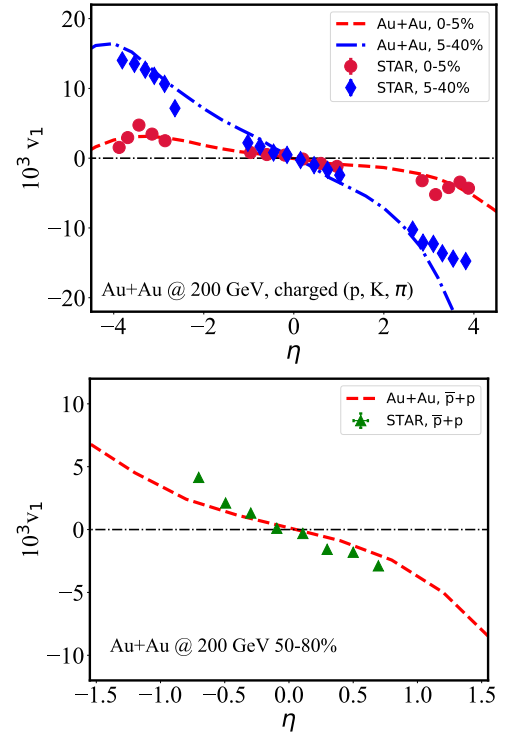


FIG. 7: (Color online) Pseudorapidity dependence of the directed flow of identified hadrons in 0-5%, 5-40% (upper panel) and 50-80% (lower panel) Au+Au collisions at  $\sqrt{s_{\text{NN}}} = 200$  GeV, compared between the CLVisc hydrodynamic calculation with the STAR data [72, 73].

In Fig 6, we show the pseudorapidity distribution of the charged particles in Au+Au, Ru+Ru and Zr+Zr collisions at  $\sqrt{s_{\text{NN}}} = 200$  GeV. As discussed in Sec. II A, the hydrodynamic model parameters summarized in Tab. II are adjusted to describe the charged light hadrons distributions in the most central collisions. As shown in the figures, our calculation presents reasonable descriptions of the PHOBOS data for Au+Au collisions on the  $dN_{\text{ch}}/d\eta$  distributions in several centralities at  $\sqrt{s_{\text{NN}}} = 200$  GeV. The results of  $dN_{\text{ch}}/d\eta$  for isobar collisions are presented and compared with the STAR data at  $\sqrt{s_{\text{NN}}} = 200$  GeV in different centralities, too. In addition, we note that the parameter  $H_i$  only affect the deformation of the medium geometry, but have very weak impact on the  $dN_{\text{ch}}/d\eta$  distributions [75]. This provides a reliable baseline for our further investigation of the light hadron directed flow.

We then present the identified particle directed flow  $v_1$  as functions of pseudorapidity. Following our previous work [74, 75], here  $v_1(\eta)$  is calculated via

$$v_1(\eta) = \langle \cos(\phi - \Psi_1) \rangle = \frac{\int \cos(\phi - \Psi_1) \frac{dN}{d\eta d\phi} d\phi}{\int \frac{dN}{d\eta d\phi} d\phi}, \quad (16)$$

where  $\Psi_1$  is the first-order event plane of the collision [45]. The directed flow coefficients are analyzed with soft hadrons within  $0 < p_{\text{T}} < 3.0$  GeV. In this work, we use the optical

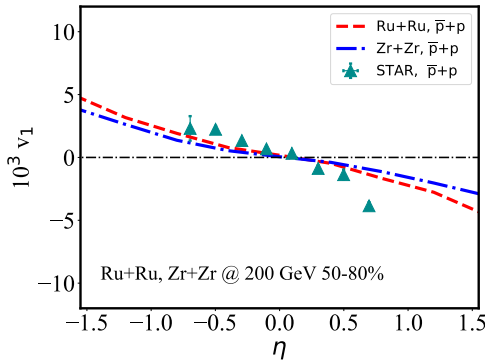


FIG. 8: (Color online) Pseudorapidity dependence of the directed flow coefficient in 50-80% Ru+Ru and Zr+Zr collisions at  $\sqrt{s_{\text{NN}}} = 200$  GeV, compared between the CLVisc hydrodynamic calculation with Case-1 nuclear structure and the STAR data [73].

Glauber model to construct the initial energy density distribution of the nuclear matter, the initial event-by-event fluctuations are neglected [45, 74]. As a result, the event plane here is same as the spectator plane determined using the deflected neutrons in realistic experimental measurements. A more consistent study will be conducted in our future work after event-by-event fluctuations are introduced.

Using above setups, we show the light hadrons  $v_1$  in Au+Au collisions for different centrality classes at  $\sqrt{s_{\text{NN}}} = 200$  GeV in Fig. 7, upper panel for charged particles and lower for proton ( $p$ ) and anti-proton ( $\bar{p}$ ). We observe our calculations for charged particle  $v_1$  within  $-4.5 < \eta < 4.5$  is consistent with the STAR data. As expected, the distribution of the identified particles  $v_1$  is consistent with that of the average flow velocity  $v_x$  of the nuclear matter.

For isobar collisions, as illustrated in Fig. 8, within our hydrodynamic framework, we are able to describe the directed flow  $v_1$  of protons ( $p^\pm$ ) at either Ru+Ru or Zr+Zr by adjusting the  $H_t$  parameter. One observes that the  $v_1$  value between two nuclei is lesser than 0.001 within  $|\eta| < 1.5$ . If one decreases the value of  $H_t$ , the slope of  $v_1$  vs.  $\eta$  will decrease near the mid-pseudorapidity region and further deviate from the experimental data. This implies the importance of the deformation of the tilted initial energy density distribution in understanding the  $\eta$ -dependence of light hadron  $v_1$  observed in experiments.

	Case-1		Case-2		Case-3	
Parameters	Ru+Ru	Zr+Zr	Ru+Ru	Zr+Zr	Ru+Ru	Zr+Zr
$R$ (fm)	5.067	4.965	5.085	5.02	5.085	5.02
$d$ (fm)	0.500	0.556	0.46	0.46	0.46	0.46
$\beta_2$	0.0	0.0	0.158	0.08	0.053	0.217

TABLE III: Nuclear structure parameters for  $^{96}_{44}\text{Ru}$  and  $^{96}_{40}\text{Zr}$  from Ref. [52].

So far, we have focused on the discussion of spherical nuclei (from DFT) in which the quadruple deformity parameter  $\beta_2 = 0.0$  (as listed in Tab. I). As pointed in Refs. [57, 59–

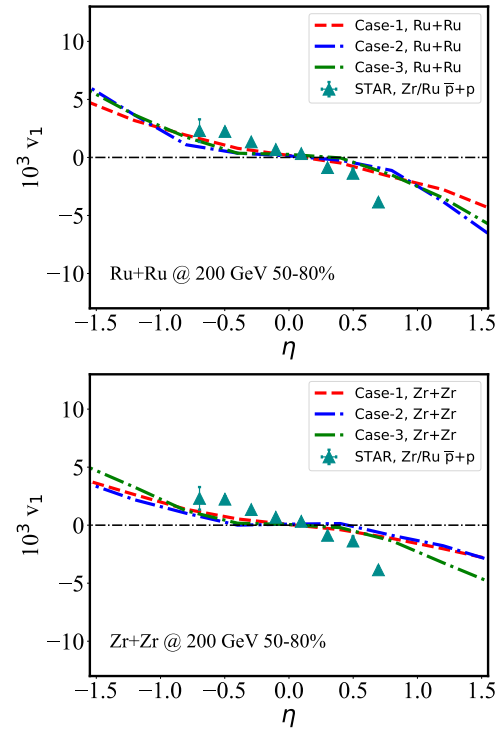


FIG. 9: (Color online) Pseudorapidity dependence of the directed flow coefficient in 50-80% Ru+Ru collisions (upper panel) and Zr+Zr collisions (lower panel) at  $\sqrt{s_{\text{NN}}} = 200$  GeV, compared between the CLVisc hydrodynamic calculation with three nuclear structure setups and the STAR data [73].

65], the elliptic flow in the most central collisions is sensitive to nuclear deformation, as deformed nuclei colliding at impact parameter  $b = 0.0$  can induce a large eccentricity on the collision orientation. In order to study the effect of nuclear deformation on light hadrons  $v_1$ , within our hydrodynamic framework, the extended WS parameters of nuclei listed in Tab. III is utilized. The two sets (Case-2 and Case-3) have the same  $R$  and  $a$  parameters and different deformations of which are constrained by  $e+A$  scattering experiments and calculations based on a finite-range droplet macroscopic model [92, 93] and the folded-Yukawa single-particle microscopic model [94]. Because of the additional protons of  $^{96}_{44}\text{Ru}$ , the charge radius of  $^{96}_{44}\text{Ru}$  is larger than that of  $^{96}_{40}\text{Zr}$ , so Ru is larger than Zr. Other parameters during the QGP evolution is as same as the spherical nuclei (Case-1).

Fig. 9 show the protons  $v_1$  in Ru+Ru/Zr+Zr collisions at  $\sqrt{s_{\text{NN}}} = 200$  GeV with various combinations of Ru and Zr deformities. The comparison between the three nuclear structure shows that the  $\beta_2$  deformations is indeed essential to change the  $v_1$  slope and magnitude at central pseudorapidity ( $|\eta| < 0.5$ ), and non-zero  $\beta_2$  further deviate from the STAR data. We see that the slope of  $v_1$  changes insignificant due to the finite  $\beta_2$  between Case-2 and Case-3 for both Ru+Ru and Zr+Zr collisions. The impact of different parameters  $R$ ,  $d$  and  $\beta_2$  on protons  $v_1$  implies that the nuclear structure slightly affect the collective flow of the final state particles. We note here

that the  $v_1$  ratio between Ru and Zr at large pseudo-rapidity may be sensitive to the nuclear structure and are not the focus of our present study on the origin of directed flow and will be left for a future investigation.

We note that since we use the optical Glauber model (smooth initial condition), our calculation is restricted to the rapidity-odd component of light hadron  $v_1$  here. The rapidity-even component  $v_1^{\text{even}}$ , including its non-trivial  $p_T$  dependence [95–97] is beyond the scope of this study and will be investigated in an upcoming effort.

#### IV. SUMMARY

In this work, we present a systematic study on how the initial medium profile of nuclei evolves to the light hadrons directed flow in heavy ion collisions. Three different nucleus-nucleus collisions –Au+Au, Ru+Ru and Zr+Zr– are compared for the tilted initial energy density distribution, and their subsequent space-time evolutions are simulated utilizing the hydrodynamic model CLVisc.

Using our realistic hydrodynamic simulation, we find that the Au+Au and isobar semi-central collisions, generates an imbalance between forward/backward moving nuclei, induces a counter-clockwise tilt of the initial medium profile in the  $x$ - $\eta_s$  plane, and induces a non-zero average pressure gradient  $-\langle \partial_x P \rangle$  with respect to time at backward/forward rapidity. Since the magnitude of pressure gradient is different at same  $|\eta_s|$  for different nucleus, which further produces a negative slope of the average QGP flow velocity  $\langle v_x \rangle$ , and in the end the same distribution of  $v_1$  vs.  $\eta$  of the final-state light hadrons. A comparison to the RHIC-STAR data indicates that the tilted initial energy density profile (or fireball geometry) is an essential factor to generate the observed light hadrons  $v_1$  in Au+Au and isobar collisions at  $\sqrt{s_{\text{NN}}} = 200$  GeV. We further find the effect of nuclear structure insignificantly affects the

light hadron directed flow at middle rapidity.

Our study provide a step forward in understanding of the origin of the light hadrons directed flow that generated in Au+Au and isobar collisions. However, in addition to the effect of tilted initial energy density, other sources also contributing to the size and sign of directed flow. For example, (1) The extremely strong electromagnetic field produced in the non-central nucleus-nucleus collisions results in directional drift of charged quarks ( $u, d, s$ ) and influence the charged particle  $v_1$  [98–100], although this effect is suggested smaller than the effect of initial tilted geometry, it is important to understand the splitting of  $v_1$  for identified light hadrons in isobar collisions [98]. (2) the fluid velocity field could provide additional contribution to the light hadrons directed flow [48]. In particular, they could affect the initial baryon density distribution and thus the nuclear matter properties [45]. (3) The light hadrons  $v_1$  can also be affected by the nuclear stopping effect and hadronic cascade after the QGP evolution, especially at lower collision energy [47, 48, 51]. These should be investigated in our future study for a more exactly understanding of the directed flow.

#### Acknowledgments

We are grateful for helpful discussions with Xiangyu Wu and Shanshan Cao. This work was supported by the National Natural Science Foundation of China (NSFC) under Grant Nos. 11935007, Guangdong Major Project of Basic and Applied Basic Research No. 2020B0301030008, the Natural Science Foundation of Hubei Province No. 2021CFB272, the the Education Department of Hubei Province of China with Young Talents Project No. Q20212703, the Open Foundation of Key Laboratory of Quark and Lepton Physics (MOE) No. QLPL202104 and the Xiaogan Natural Science Foundation under Grant No. XGKJ2021010016.

- 
- [1] S. S. Adler et al. Elliptic flow of identified hadrons in Au+Au collisions at  $\sqrt{s_{\text{NN}}} = 200$ -GeV. *Phys. Rev. Lett.*, 91:182301, 2003.
  - [2] K. Aamodt et al. Elliptic flow of charged particles in Pb-Pb collisions at 2.76 TeV. *Phys. Rev. Lett.*, 105:252302, 2010.
  - [3] S. Chatrchyan et al. Measurement of the elliptic anisotropy of charged particles produced in PbPb collisions at  $\sqrt{s_{\text{NN}}} = 2.76$  TeV. *Phys. Rev. C*, 87(1):014902, 2013.
  - [4] Jean-Yves Ollitrault. Anisotropy as a signature of transverse collective flow. *Phys. Rev. D*, 46:229–245, 1992.
  - [5] Dirk H. Rischke, S. Bernard, and J. A. Maruhn. Relativistic hydrodynamics for heavy ion collisions. I. General aspects and expansion into vacuum. *Nucl. Phys. A*, 595:346–382, 1995.
  - [6] H. Sorge. Elliptical flow: A Signature for early pressure in ultrarelativistic nucleus-nucleus collisions. *Phys. Rev. Lett.*, 78:2309–2312, 1997.
  - [7] S.A. Bass, M. Gyulassy, H. Stoecker, and W. Greiner. Signatures of quark gluon plasma formation in high-energy heavy ion collisions: A Critical review. *J. Phys. G*, 25:R1–R57, 1999.
  - [8] C. E. Aguiar, Y. Hama, T. Kodama, and T. Osada. Event-by-event fluctuations in hydrodynamical description of heavy ion collisions. *Nucl. Phys. A*, 698:639–642, 2002.
  - [9] E. Shuryak. Why does the quark gluon plasma at RHIC behave as a nearly ideal fluid? *Prog. Part. Nucl. Phys.*, 53:273–303, 2004.
  - [10] M. Gyulassy and L. McLerran. New forms of QCD matter discovered at RHIC. *Nucl. Phys. A*, 750:30–63, 2005.
  - [11] W. Broniowski, P. Bozek, and M. Rybczynski. Fluctuating initial conditions in heavy-ion collisions from the Glauber approach. *Phys. Rev. C*, 76:054905, 2007.
  - [12] R. P. G. Andrade, F. Grassi, Y. Hama, T. Kodama, and W. L. Qian. Importance of Granular Structure in the Initial Conditions for the Elliptic Flow. *Phys. Rev. Lett.*, 101:112301, 2008.
  - [13] T. Hirano and Y. Nara. Eccentricity fluctuation effects on elliptic flow in relativistic heavy ion collisions. *Phys. Rev. C*, 79:064904, 2009.
  - [14] B. Schenke, Sangyong Jeon, and C. Gale. Elliptic and triangular flow in event-by-event (3+1)D viscous hydrodynamics.

- Phys. Rev. Lett.*, 106:042301, 2011.
- [15] Zhi Qiu and Ulrich W. Heinz. Event-by-event shape and flow fluctuations of relativistic heavy-ion collision fireballs. *Phys. Rev. C*, 84:024911, 2011.
- [16] U. Heinz and R. Snellings. Collective flow and viscosity in relativistic heavy-ion collisions. *Ann. Rev. Nucl. Part. Sci.*, 63:123–151, 2013.
- [17] P. Huovinen. Hydrodynamics at RHIC and LHC: What have we learned? *Int. J. Mod. Phys. E*, 22:1330029, 2013.
- [18] C. Gale, Sangyong Jeon, and B. Schenke. Hydrodynamic Modeling of Heavy-Ion Collisions. *Int. J. Mod. Phys. A*, 28:1340011, 2013.
- [19] P. Bozek and W. Broniowski. Collective dynamics in high-energy proton-nucleus collisions. *Phys. Rev. C*, 88(1):014903, 2013.
- [20] Guang-You Qin and B. Müller. Elliptic and triangular flow anisotropy in deuteron-gold collisions at  $\sqrt{s_{NN}} = 200$  GeV at RHIC and in proton-lead collisions at  $\sqrt{s_{NN}} = 5.02$  TeV at the LHC. *Phys. Rev. C*, 89(4):044902, 2014.
- [21] K. Dusling, Wei Li, and B. Schenke. Novel collective phenomena in high-energy proton-proton and proton-nucleus collisions. *Int. J. Mod. Phys. E*, 25(01):1630002, 2016.
- [22] P. Romatschke and U. Romatschke. *Relativistic Fluid Dynamics In and Out of Equilibrium*. Cambridge Monographs on Mathematical Physics. Cambridge University Press, 5 2019.
- [23] R. D. Weller and P. Romatschke. One fluid to rule them all: viscous hydrodynamic description of event-by-event central p+p, p+Pb and Pb+Pb collisions at  $\sqrt{s} = 5.02$  TeV. *Phys. Lett. B*, 774:351–356, 2017.
- [24] Wenbin Zhao, Che Ming Ko, Yu-Xin Liu, Guang-You Qin, and Huichao Song. Probing the Partonic Degrees of Freedom in High-Multiplicity  $p - Pb$  collisions at  $\sqrt{s_{NN}} = 5.02$  TeV. *Phys. Rev. Lett.*, 125(7):072301, 2020.
- [25] Huichao Song, Steffen A. Bass, Ulrich Heinz, Tetsufumi Hirano, and Chun Shen. 200 A GeV Au+Au collisions serve a nearly perfect quark-gluon liquid. *Phys. Rev. Lett.*, 106:192301, 2011. [Erratum: *Phys.Rev.Lett.* 109, 139904 (2012)].
- [26] Jonah E. Bernhard, J. Scott Moreland, and Steffen A. Bass. Bayesian estimation of the specific shear and bulk viscosity of quark-gluon plasma. *Nature Phys.*, 15(11):1113–1117, 2019.
- [27] M. Gyulassy, K. A. Frankel, and Horst Stoecker. DO NUCLEI FLOW AT HIGH-ENERGIES? *Phys. Lett. B*, 110:185–188, 1982.
- [28] H. A. Gustafsson et al. Collective Flow Observed in Relativistic Nuclear Collisions. *Phys. Rev. Lett.*, 52:1590–1593, 1984.
- [29] Michael Annan Lisa, Ulrich W. Heinz, and Urs Achim Wiedemann. Tilted pion sources from azimuthally sensitive HBT interferometry. *Phys. Lett. B*, 489:287–292, 2000.
- [30] S. Voloshin and Y. Zhang. Flow study in relativistic nuclear collisions by Fourier expansion of Azimuthal particle distributions. *Z. Phys. C*, 70:665–672, 1996.
- [31] A. Bilandzic, R. Snellings, and S. Voloshin. Flow analysis with cumulants: Direct calculations. *Phys. Rev. C*, 83:044913, 2011.
- [32] J. Adams et al. Azimuthal anisotropy in Au+Au collisions at  $s(NN)^{1/2} = 200$ -GeV. *Phys. Rev. C*, 72:014904, 2005.
- [33] L. Adamczyk et al. Beam-Energy Dependence of the Directed Flow of Protons, Antiprotons, and Pions in Au+Au Collisions. *Phys. Rev. Lett.*, 112(16):162301, 2014.
- [34] L. Adamczyk et al. Beam-Energy Dependence of Directed Flow of  $\Lambda$ ,  $\bar{\Lambda}$ ,  $K^\pm$ ,  $K_s^0$  and  $\phi$  in Au+Au Collisions. *Phys. Rev. Lett.*, 120(6):062301, 2018.
- [35] J. Adam et al. First Observation of the Directed Flow of  $D^0$  and  $\bar{D}^0$  in Au+Au Collisions at  $\sqrt{s_{NN}} = 200$  GeV. *Phys. Rev. Lett.*, 123(16):162301, 2019.
- [36] S. Acharya et al. Probing the effects of strong electromagnetic fields with charge-dependent directed flow in Pb-Pb collisions at the LHC. *Phys. Rev. Lett.*, 125(2):022301, 2020.
- [37] Jaroslav Adam et al. Bulk properties of the system formed in Au + Au collisions at  $\sqrt{s_{NN}} = 14.5$  GeV at the BNL STAR detector. *Phys. Rev. C*, 101(2):024905, 2020.
- [38] S. Singha, P. Shanmuganathan, and D. Keane. The first moment of azimuthal anisotropy in nuclear collisions from AGS to LHC energies. *Adv. High Energy Phys.*, 2016:2836989, 2016.
- [39] Y. Nara, H. Niemi, A. Ohnishi, and H. Stöcker. Examination of directed flow as a signature of the softest point of the equation of state in QCD matter. *Phys. Rev. C*, 94(3):034906, 2016.
- [40] S. Chatterjee and P. Bozek. Large directed flow of open charm mesons probes the three dimensional distribution of matter in heavy ion collisions. *Phys. Rev. Lett.*, 120(19):192301, 2018.
- [41] Chao Zhang, Jiamin Chen, Xiaofeng Luo, Feng Liu, and Y. Nara. Beam energy dependence of the squeeze-out effect on the directed and elliptic flow in Au + Au collisions in the high baryon density region. *Phys. Rev. C*, 97(6):064913, 2018.
- [42] Chong-Qiang Guo, Chun-Jian Zhang, and Jun Xu. Revisiting directed flow in relativistic heavy-ion collisions from a multiphase transport model. *Eur. Phys. J. A*, 53(12):233, 2017.
- [43] Tribhuban Parida and Sandeep Chatterjee. Splitting of elliptic flow in a tilted fireball. *arXiv: 2204.02345*.
- [44] A. Adil and M. Gyulassy. 3D jet tomography of twisted strongly coupled quark gluon plasmas. *Phys. Rev. C*, 72:034907, 2005.
- [45] P. Bozek and I. Wyskiel. Directed flow in ultrarelativistic heavy-ion collisions. *Phys. Rev. C*, 81:054902, 2010.
- [46] Baoyi Chen, Maoxin Hu, Huanyu Zhang, and Jiaying Zhao. Probe the tilted Quark-Gluon Plasma with charmonium directed flow. *Phys. Lett. B*, 802:135271, 2020.
- [47] Chun Shen and S. Alzhrani. Collision-geometry-based 3D initial condition for relativistic heavy-ion collisions. *Phys. Rev. C*, 102(1):014909, 2020.
- [48] Sangwook Ryu, Vahidin Jupic, and Chun Shen. Probing early-time longitudinal dynamics with the  $\Lambda$  hyperon's spin polarization in relativistic heavy-ion collisions. *Phys. Rev. C*, 104(5):054908, 2021.
- [49] S. Chatterjee and P. Bozek. Interplay of drag by hot matter and electromagnetic force on the directed flow of heavy quarks. *Phys. Lett. B*, 798:134955, 2019.
- [50] A. Beraudo, A. De Pace, M. Monteno, M. Nardi, and F. Prino. Rapidity dependence of heavy-flavour production in heavy-ion collisions within a full 3+1 transport approach: quenching, elliptic and directed flow. *JHEP*, 05:279, 2021.
- [51] Piotr Bozek. Splitting of proton-antiproton directed flow in relativistic heavy-ion collisions. *arXiv: 2207.04927*.
- [52] Mohamed Abdallah et al. Search for the chiral magnetic effect with isobar collisions at  $\sqrt{s_{NN}}=200$  GeV by the STAR Collaboration at the BNL Relativistic Heavy Ion Collider. *Phys. Rev. C*, 105(1):014901, 2022.
- [53] Kenji Fukushima, Dmitri E. Kharzeev, and Harmen J. Warringa. The Chiral Magnetic Effect. *Phys. Rev. D*, 78:074033, 2008.
- [54] V. Skokov, A. Yu. Illarionov, and V. Toneev. Estimate of the magnetic field strength in heavy-ion collisions. *Int. J. Mod. Phys. A*, 24:5925–5932, 2009.
- [55] Wei-Tian Deng, Xu-Guang Huang, Guo-Liang Ma, and Gang Wang. Test the chiral magnetic effect with isobaric collisions. *Phys. Rev. C*, 94:041901, 2016.

- [56] Xin-Li Zhao, Guo-Liang Ma, and Yu-Gang Ma. Impact of magnetic-field fluctuations on measurements of the chiral magnetic effect in collisions of isobaric nuclei. *Phys. Rev. C*, 99(3):034903, 2019.
- [57] Govert Nijs and Wilke van der Schee. Inferring nuclear structure from heavy isobar collisions using Trajectum. *arXiv: 2112.13771*.
- [58] Chunjian Zhang, Somadutta Bhatta, and Jianguyong Jia. Ratios of collective flow observables in high-energy isobar collisions are insensitive to final state interactions. *arXiv: 2206.01943*.
- [59] Chunjian Zhang and Jianguyong Jia. Evidence of Quadrupole and Octupole Deformations in Zr96+Zr96 and Ru96+Ru96 Collisions at Ultrarelativistic Energies. *Phys. Rev. Lett.*, 128(2):022301, 2022.
- [60] Jianguyong Jia and Chun-Jian Zhang. Scaling approach to nuclear structure in high-energy heavy-ion collisions. *arXiv: 2111.15559*.
- [61] Hao-jie Xu, Wenbin Zhao, Hanlin Li, Ying Zhou, Lie-Wen Chen, and Fuqiang Wang. Probing nuclear structure with mean transverse momentum in relativistic isobar collisions. *arXiv: 2111.14812*.
- [62] Fei Li, Yu-Gang Ma, Song Zhang, Guo-Liang Ma, and Qi-Ye Shou. Impact of nuclear structure on the CME background in  $^{96}_{44}\text{Ru} + ^{96}_{44}\text{Ru} + ^{96}_{40}\text{Zr} + ^{96}_{40}\text{Zr}$  collisions at  $\sqrt{s_{NN}} = 7.7 \sim 200$  GeV from a multiphase transport model. *arXiv: 2201.10994*.
- [63] Xin-Li Zhao and Guo-Liang Ma. Search for the chiral magnetic effect in collisions between two isobars with nuclear structures. *arXiv: 2203.15214*.
- [64] Yu-Gang Ma and Song Zhang. Influence of nuclear structure in relativistic heavy-ion collisions. *arXiv: 2206.08218*.
- [65] Jianguyong Jia, Giuliano Giacalone, and Chunjian Zhang. Precision tests of the nonlinear mode coupling of anisotropic flow via high-energy collisions of isobars. *arXiv: 2206.07184*.
- [66] Long-Gang Pang, H. Petersen, Qun Wang, and Xin-Nian Wang. Vortical Fluid and  $\Lambda$  Spin Correlations in High-Energy Heavy-Ion Collisions. *Phys. Rev. Lett.*, 117(19):192301, 2016.
- [67] Long-Gang Pang, H. Petersen, and Xin-Nian Wang. Pseudorapidity distribution and decorrelation of anisotropic flow within the open-computing-language implementation CLVisc hydrodynamics. *Phys. Rev. C*, 97(6):064918, 2018.
- [68] Xiang-Yu Wu, Long-Gang Pang, Guang-You Qin, and Xin-Nian Wang. Longitudinal fluctuations and decorrelations of anisotropic flows at energies available at the CERN Large Hadron Collider and at the BNL Relativistic Heavy Ion Collider. *Phys. Rev. C*, 98(2):024913, 2018.
- [69] Hao-Jie Xu, Xiaobao Wang, Hanlin Li, Jie Zhao, Zi-Wei Lin, Caiwan Shen, and Fuqiang Wang. Importance of isobar density distributions on the chiral magnetic effect search. *Phys. Rev. Lett.*, 121(2):022301, 2018.
- [70] Hanlin Li, Hao-jie Xu, Jie Zhao, Zi-Wei Lin, Hanzhong Zhang, Xiaobao Wang, Caiwan Shen, and Fuqiang Wang. Multiphase transport model predictions of isobaric collisions with nuclear structure from density functional theory. *Phys. Rev. C*, 98(5):054907, 2018.
- [71] Hao-jie Xu, Hanlin Li, Xiaobao Wang, Caiwan Shen, and Fuqiang Wang. Determine the neutron skin type by relativistic isobaric collisions. *Phys. Lett. B*, 819:136453, 2021.
- [72] B.I. Abelev et al. System-size independence of directed flow at the Relativistic Heavy-Ion Collider. *Phys. Rev. Lett.*, 101:252301, 2008.
- [73] A. I. Sheikh for the STAR Collaboration. Splitting of directed flow for identified light hadrons ( $\pi$ , K, p) and strange baryons ( $\Xi$ ,  $\Omega$ ) in Au+Au and isobar collisions at STAR. *29th Conference on Ultra-relativistic Nucleus-Nucleus Collisions – Quark Matter 2022*.
- [74] Ze-Fang Jiang, C. B. Yang, and Qi Peng. Directed flow of charged particles within idealized viscous hydrodynamics at energies available at the BNL Relativistic Heavy Ion Collider and at the CERN Large Hadron Collider. *Phys. Rev. C*, 104(6):064903, 2021.
- [75] Ze-Fang Jiang, Shanshan Cao, Xiang-Yu Wu, C. B. Yang, and Ben-Wei Zhang. Longitudinal distribution of initial energy density and directed flow of charged particles in relativistic heavy-ion collisions. *Phys. Rev. C*, 105(3):034901, 2022.
- [76] Ze-Fang Jiang, Shanshan Cao, Wen-Jing Xing, Xiang-Yu Wu, C. B. Yang, and Ben-Wei Zhang. Probing the initial longitudinal density profile and electromagnetic field in ultrarelativistic heavy-ion collisions with heavy quarks. *Phys. Rev. C*, 105(5):054907, 2022.
- [77] Xiaowen Li, Ze-Fang Jiang, Shanshan Cao, and Jian Deng. Evolution of global polarization in relativistic heavy-ion collisions within a perturbative approach. *arXiv: 2205.02409*.
- [78] Wei-Tian Deng, Xu-Guang Huang, Guo-Liang Ma, and Gang Wang. Predictions for isobaric collisions at  $\sqrt{s_{NN}} = 200$  GeV from a multiphase transport model. *Phys. Rev. C*, 97(4):044901, 2018.
- [79] C. Loizides, J. Kamin, and D. d’Enterria. Improved Monte Carlo Glauber predictions at present and future nuclear colliders. *Phys. Rev. C*, 97(5):054910, 2018. [Erratum: Phys.Rev.C 99, 019901 (2019)].
- [80] Piotr Bozek. Flow and interferometry in 3+1 dimensional viscous hydrodynamics. *Phys. Rev. C*, 85:034901, 2012.
- [81] Wei Chen, Shanshan Cao, Tan Luo, Long-Gang Pang, and Xin-Nian Wang. Effects of jet-induced medium excitation in  $\gamma$ -hadron correlation in A+A collisions. *Phys. Lett. B*, 777:86–90, 2018.
- [82] Yayun He, Long-Gang Pang, and Xin-Nian Wang. Bayesian extraction of jet energy loss distributions in heavy-ion collisions. *Phys. Rev. Lett.*, 122(25):252302, 2019.
- [83] Ze Fang Jiang, Duan She, C.B. Yang, and Defu Hou. Perturbation solutions of relativistic viscous hydrodynamics for longitudinally expanding fireballs. *Chin. Phys. C*, 44(8):084107, 2020.
- [84] Ze Fang Jiang, C.B. Yang, Chi Ding, and Xiang-Yu Wu. Pseudo-rapidity distribution from a perturbative solution of viscous hydrodynamics for heavy ion collisions at RHIC and LHC. *Chin. Phys. C*, 42(12):123103, 2018.
- [85] G.S. Denicol, H. Niemi, E. Molnar, and D.H. Rischke. Derivation of transient relativistic fluid dynamics from the Boltzmann equation. *Phys. Rev. D*, 85:114047, 2012. [Erratum: Phys.Rev.D 91, 039902 (2015)].
- [86] P. Romatschke. New Developments in Relativistic Viscous Hydrodynamics. *Int. J. Mod. Phys. E*, 19:1–53, 2010.
- [87] S. Borsanyi, Z. Fodor, C. Hoelbling, S. D. Katz, S. Krieg, and K. K. Szabo. Full result for the QCD equation of state with 2+1 flavors. *Phys. Lett. B*, 730:99–104, 2014.
- [88] Wenbin Zhao, Weiyao Ke, Wei Chen, Tan Luo, and Xin-Nian Wang. From Hydrodynamics to Jet Quenching, Coalescence, and Hadron Cascade: A Coupled Approach to Solving the RAA $\otimes$ v2 Puzzle. *Phys. Rev. Lett.*, 128(2):022302, 2022.
- [89] Xiang-Yu Wu, Guang-You Qin, Long-Gang Pang, and Xin-Nian Wang. (3+1)-D viscous hydrodynamics at finite net baryon density: Identified particle spectra, anisotropic flows, and flow fluctuations across energies relevant to the beam-energy scan at RHIC. *Phys. Rev. C*, 105(3):034909, 2022.
- [90] F. Cooper and G. Frye. Comment on the Single Particle Distribution in the Hydrodynamic and Statistical Thermodynamic Models of Multiparticle Production. *Phys. Rev. D*, 10:186,

- 1974.
- [91] B. Alver et al. Phobos results on charged particle multiplicity and pseudorapidity distributions in Au+Au, Cu+Cu, d+Au, and p+p collisions at ultra-relativistic energies. *Phys. Rev. C*, 83:024913, 2011.
- [92] S. Raman, C. W. G. Nestor, Jr, and P. Tikkanen. Transition probability from the ground to the first-excited  $2^+$  state of even-even nuclides. *Atom. Data Nucl. Data Tabl.*, 78:1–128, 2001.
- [93] B. Pritychenko, M. Birch, B. Singh, and M. Horoi. Tables of E2 Transition Probabilities from the first  $2^+$  States in Even-Even Nuclei. *Atom. Data Nucl. Data Tabl.*, 107:1–139, 2016. [Erratum: *Atom. Data Nucl. Data Tabl.* 114, 371–374 (2017)].
- [94] P. Moller, J. R. Nix, W. D. Myers, and W. J. Swiatecki. Nuclear ground state masses and deformations. *Atom. Data Nucl. Data Tabl.*, 59:185–381, 1995.
- [95] Derek Teaney and Li Yan. Triangularity and Dipole Asymmetry in Heavy Ion Collisions. *Phys. Rev. C*, 83:064904, 2011.
- [96] Matthew Luzum and Jean-Yves Ollitrault. Directed flow at midrapidity in heavy-ion collisions. *Phys. Rev. Lett.*, 106:102301, 2011.
- [97] Charles Gale, Sangyong Jeon, Björn Schenke, Prithwish Tribedy, and Raju Venugopalan. Event-by-event anisotropic flow in heavy-ion collisions from combined Yang-Mills and viscous fluid dynamics. *Phys. Rev. Lett.*, 110(1):012302, 2013.
- [98] G. Inghirami, M. Mace, Y. Hirono, L. Del Zanna, D. E. Kharzeev, and M. Bleicher. Magnetic fields in heavy ion collisions: flow and charge transport. *Eur. Phys. J. C*, 80(3):293, 2020.
- [99] U. Gürsoy, D. E. Kharzeev, and K. Rajagopal. Magnetohydrodynamics, charged currents and directed flow in heavy ion collisions. *Phys. Rev. C*, 89(5):054905, 2014.
- [100] U. Gürsoy, D. E. Kharzeev, E. Marcus, K. Rajagopal, and Chun Shen. Charge-dependent Flow Induced by Magnetic and Electric Fields in Heavy Ion Collisions. *Phys. Rev. C*, 98(5):055201, 2018.
- [101] S.A. Bass et al. Microscopic models for ultrarelativistic heavy ion collisions. *Prog. Part. Nucl. Phys.*, 41:255–369, 1998.
- [102] H. Petersen, D. Oliinychenko, M. Mayer, J. Staudenmaier, and S. Ryu. SMASH – A new hadronic transport approach. *Nucl. Phys. A*, 982:399–402, 2019.